Femtosecond carrier dynamics in graphite

K. Seibert, G. C. Cho, W. Kütt, and H. Kurz
Institute of Semiconductor Electronics, Rheinisch-Westfälische Technische Hochschule Aachen, D-5100 Aachen, Federal Republic of Germany

D. H. Reitze, J. I. Dadap, H. Ahn, and M. C. Downer
Department of Physics, The University of Texas at Austin, Austin, Texas 78712-1081

A. M. Malvezzi
Department of Electronics, University of Pavia, I-27100 Pavia, Italy
(Received 9 February 1990; revised manuscript received 25 April 1990)

We present a comprehensive report of pump-probe reflectivity and transmission measurements on highly oriented pyrolytic graphite with 50 fs time resolution. The experiments trace the generation, relaxation, and recombination of nonequilibrium carriers in a quasi-two-dimensional semimetallic solid over a wide range of experimental parameters. The fluence of excitation at $h\nu=2.0$ eV was varied between 10^{-6} and 10^{-2} J/cm^2, below the threshold for optical damage, while probe pulses in the photon energy range $1.5<h\nu<4.0$ eV were used. On a subpicosecond time scale we observe a strong, initial, broadband absorption saturation caused by state filling by a hot, dense π-band electron population, which recovers with a fluence- and probe-wavelength-dependent time constant as the carriers cool and recombine in less than 1 ps. Later dynamics reflect the generation and diffusion of heat in the lattice, and are consistent with previous picosecond reflectivity measurements.

I. INTRODUCTION

Because of its simple quasi-two-dimensional structure, and because of the availability of good-quality crystalline samples, graphite has served as a "textbook" system for fundamental investigations of solid-state physics of all kinds for over 50 years.[1] For example, graphite was one of the earliest materials to which the quantum theory of solid-state band structure was applied.[2] Subsequently these band-structure calculations have been greatly refined, and related in detail to the equilibrium electronic and optical properties of graphite.[3,4] Nevertheless very little is known about the ultrafast dynamics of nonequilibrium electronic carriers in graphite, despite extensive investigations of such processes in other materials using the techniques of ultrafast laser spectroscopy.[5] Indeed, because of its well-characterized, highly anisotropic, semimetallic properties, graphite provides an excellent opportunity to study fundamental femtosecond solid-state processes possessing both major differences from, as well as important similarities to, related processes in isotropic semiconductors and metals, which have been the dominant focus of ultrafast spectroscopy of solids for the past several years.[5]

In this paper we report the first femtosecond time-resolved study of the generation, relaxation, and recombination of nonequilibrium electronic carriers in solid graphite over a wide range of optical excitation conditions below the threshold for optical damage. Our experiments utilize a pump and probe technique with 50-fs time resolution, and examine both the time-resolved reflectivity of bulk samples and time-resolved transmission through thin films in order to characterize the evolving optical properties as completely as possible. The results show clearly that important initial stages of the dynamics were beyond the resolution of previous experiments performed with picosecond pulses.[6,7] Furthermore, two fundamental properties of graphite lend the femtosecond carrier dynamics a unique character. First, its extreme anisotropy strongly suppresses carrier diffusion perpendicular to the basal planes, despite the short absorption depth and high-carrier-density gradients which are generated. Consequently, graphite is an excellent model system to study the ultrafast dynamics of a two-dimensional electron-hole plasma. Second, its semimetallic band structure introduces elements familiar from dynamics in both semiconductors and metals. Graphite shares with semiconductors the ability to generate an electron-hole plasma by optical excitation, and to follow its evolution with an optical probe. On the other hand, it shares with metals the absence of a band gap. Consequently, electron-hole recombination can occur immediately upon relaxation to the band extrema.

There is an important additional motivation behind our work. In the last few years, several studies[6-12] have shown that intense pulsed laser excitation of graphite can induce melting, even though graphite normally sublimes when heated adiabatically at subkilobar pressures. These studies have used nanosecond,[8,9] picosecond,[6,7,10,11] and very recently femtosecond[12] laser pulses to provide new, although sometimes conflicting, information on the ultrafast laser-induced melting process and on the unique material properties of liquid carbon produced by intense laser excitation. Nevertheless, the changes in optical

properties caused by ultrafast melting are convolved with changes caused by nonequilibrium carriers initially generated in the solid, especially in femtosecond experiments.[12] Consequently, the low-excitation work reported here aids the interpretation of these high-excitation experiments by helping to distinguish the effects of solid-state carriers.

II. EXPERIMENTAL PROCEDURE

Our experiments were performed with room-temperature samples of highly oriented pyrolytic graphite (HOPG). The basic material properties of these samples are described elsewhere.[1,8,9] For front-surface-reflectivity experiments, optically opaque multilayered samples were used with the surface normal to the graphite c axis. For simultaneous reflectivity-transmission experiments, thin HOPG films were prepared by peeling optically thin layers from a master sample with transparent tape. Strong light scattering was observed from the free-standing films. However, scattering was greatly reduced by gluing the films to a glass substrate before removing the tape. Mounted films were therefore used in the experiments. The experiments were performed with a standard pump-and-probe method. A dispersion-compensated, colliding-pulse, mode-locked dye laser[13] supplied optical pulses of 50-fs duration, centered at $\lambda=0.62$ μm, at a repetition rate of 100 MHz. For experiments at a low level of sample excitation, this source was used at its full repetition rate without any external amplification. Pump pulses were focused at normal incidence onto the sample surface either at the full fluence of 15 μJ/cm^2 or attenuated to as little as 1 μJ/cm^2. A train of weak probe pulses was split from the pump beam, passed through a variable optical delay, and focused tightly at near-normal incidence to a beam waist centered within the pump spot on the sample surface. The reflected and/or transmitted probe beams were detected with photodiodes as the pump-probe optical delay was varied. Standard synchronous detection methods, involving mechanical chopping of the pump beam, lock-in amplification of the modulated probe, and slow scan of the optical delay, served to enhance signal-to-noise ratio. However, at the lowest levels of excitation, superior signal-to-noise ratio and baseline stability were achieved with a novel rapid data-acquisition[14] system in which the optical delay was swept rapidly and repeatedly at up to 200 Hz repetition rate, while a specially developed computer acquired 12-bit data at a 4-MHz rate and averaged data points over as much as 10^5 scans. This resulted in a detectivity of $\Delta R/R_0$ and $\Delta T/T_0$ of a few 10^{-7}. For experiments at higher levels of excitation, the output of the colliding-pulse laser was amplified at a 7-kHz repetition rate in a multipass dye amplifier pumped by a copper-vapor laser.[15] Measurements at pump fluences up to 16 mJ/cm^2 were made with this output. In addition, the amplified output permitted a wide spectral probing range (0.84 μm$>\lambda>0.45$ μm) by generating white-light continuum-probe pulses[16] in an ethylene glycol jet. Continuum-probing measurements were done placing an interference filter with calibrated center wavelength and 10-nm bandwidth after the glycol jet to select the probe wavelength reaching the sample. Cross-correlation measurements between the 620-nm pump and respective probe pulses was accomplished by substituting a thin (<100 μm) ZnO crystal at the sample location and monitoring sum frequency absorption as a function of pump-probe time delay. The measured widths of the cross-correlation curves were approximately 130 fs at the extreme wavelengths (i.e., 450 and 800 nm) and approximately 100 fs around the central wavelength (620 nm), indicating a probe-pulse width shorter than 100 fs in the complete wavelength range. By generating second-harmonic pulses, measurements with probe pulses at $\lambda=0.31$ μm were also performed. No measurements are reported at fluences above 16 mJ/cm^2 because evidence of cumulative optical damage appeared on the sample surface. Nevertheless, independent measurements made with a 10-Hz-repetition-rate amplifier system,[12] slow enough that the sample could be translated to a fresh region in between individual laser shots, have shown that the optical response retains the same qualitative features as the data reported here for pump fluences up to the single-shot melting threshold, which was measured to occur at 130 mJ/cm^2. Thus our measurements cover a range of 5 orders of magnitude of pump fluence up to the single-shot melting threshold, above which radically different effects are observed.[12]

III. EXPERIMENTAL RESULTS

Figure 1 presents time-resolved transmission and reflectivity data recorded simultaneously from HOPG film of approximately 350 Å thickness, as estimated from the 20% transmittance of the unexcited sample. The data in Fig. 1 contrast the first picosecond of the optical response following a very low level of excitation (5 μJ/cm^2) with the response following thousandfold more intense excitation (7.5 mJ/cm^2). Pump-and-probe pulses were both at $\lambda=620$ nm ($h\nu=2.0$ eV). Transmission and reflectivity data were also taken with thicker films (~ 600 Å). Essential features of the optical response, particularly the recovery time constants, were consistent with those presented here for 350-Å films.

Figure 1(a) shows $\Delta T/T_0$ and $\Delta R/R_0$ for low excitation. The initial response is a pulsewidth-limited rise in transmission, accompanied by a simultaneous, and smaller, drop in reflectivity. These initial changes reach peak magnitude slightly after $\Delta t=0$, which was determined independently to within ± 20 fs by measuring two-photon absorption cross correlation in a thin crystalline film of GaP which was translated into the sample position. $\Delta T/T_0$ and $\Delta R/R_0$ then both recover rapidly, with a fall time $\tau=30\pm 10$ fs, determined by a fit of the data to a single-exponential response convolved with Gaussian pump-and-probe temporal profiles of 50 fs FWHM. Finally, for $\Delta t>200$ fs, there is an overshoot in both signals, $\Delta T/T_0$ dropping slightly below, and $\Delta R/R_0$ rising slightly above zero.

Figure 1(b) shows the result of converting this data into the corresponding changes $\Delta\epsilon_1/\epsilon_1$ and $\Delta\epsilon_2/\epsilon_2$ in the real and imaginary parts of the dielectric function. A de-

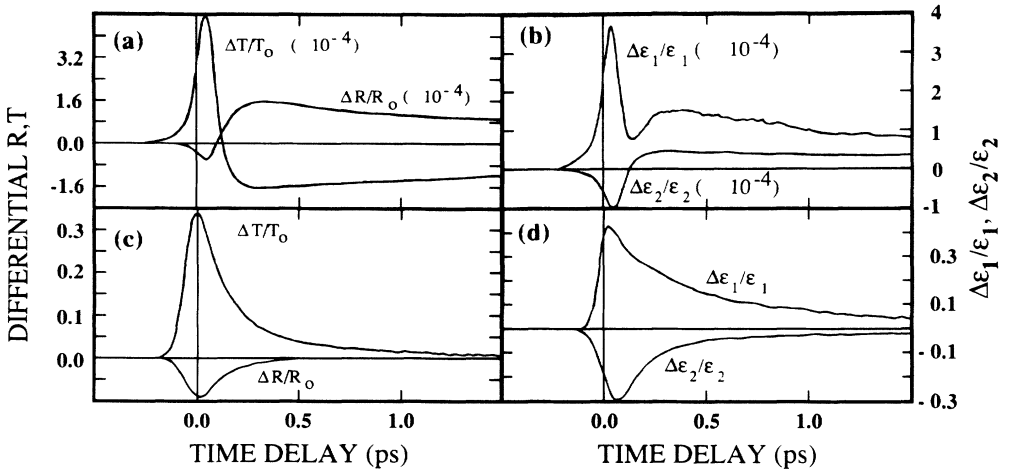

FIG. 1. Femtosecond transmission (T) and reflectivity (R) data from thin graphite films, showing the first picosecond of the optical response. (a) Pump fluence 5 μJ/cm^2, probe wavelength 0.62 μm, data taken with output of unamplified CPM laser. (b) Fractional changes in the real (ϵ_1) and imaginary (ϵ_2) parts of the complex dielectric function extracted from the data in (a). (c) Pump fluence 7.5 mJ/cm^2, probe wavelength 0.62 μm, data taken with amplified pulses. Note the longer relaxation time compared to (a). (d) Fractional changes in the dielectric function corresponding to data in (c).

crease in ϵ_2 and a simultaneous increase in ϵ_1 underlie the initial reflectivity-transmission transient. The decrease in ϵ_2 can be interpreted as a slight interband absorption saturation caused by state filling, while the accompanying change in ϵ_1 follows from the Kramers-Kronig relation. Possible causes of the changes at later time delays are discussed in the next section. All extracted $\Delta\epsilon/\epsilon$ curves presented in this paper were confirmed independently by reconstructing from them a calculated *bulk* reflectivity transient. This calculated bulk reflectivity was then compared with an actual measured reflectivity transient from a bulk sample excited at the same fluence level. In all cases, excellent agreement ($<10\%$ error in $\Delta R/R_0$ at all observed time delays) is observed in the sign and magnitude of reflectivity change. This check ensures that the determination of $\Delta\epsilon/\epsilon$ from $\Delta R/R_0$ and $\Delta T/T_0$ at one wavelength is an unambiguous procedure. The consistency of bulk and thin-film optical responses also implies that classical size effects have little impact on the measured thin-film response, and that carrier scattering at surfaces or cleavage planes, if important, influences the thin-film and bulk response in similar ways.

As pump fluence is raised to several mJ/cm^2, important changes are observed in the initial optical response, as shown in Fig. 1(c) for excitation at 7.5 mJ/cm^2. The most obvious difference is that the initial transients are much larger in magnitude, in approximate proportion to the increased pump fluence. A precise statement regarding the linear or nonlinear scaling of the $\Delta T/T_0$ and $\Delta R/R_0$ signals is difficult to make because the data in Figs. 1(a) and 1(c) were taken with different laser systems. Furthermore, somewhat different scaling of $\Delta T/T_0$ and $\Delta R/R_0$ with fluence is expected, according to the laws of thin-film optics and because of the different temporal evolution of the two signals, and is observed. Nevertheless, the peak $\Delta T/T_0$ and $\Delta R/R_0$ signals scale approximately linearly with pump fluence up to 7.5 mJ/cm^2, with perhaps a small degree of saturation as discussed further in the following section. A much more precise comparison can be made of recovery times, which at high fluence [Fig. 1(c)] are unambiguously longer than the pulse duration. A careful fit of both curves to an exponential recovery convolved with Gaussian pump and probe temporal profiles yields a decay constant $\tau=130\pm15$ fs for $\Delta T/T_0$ and $\Delta R/R_0$. The $\Delta T/T_0$ and $\Delta R/R_0$ signals eventually overshoot the original values slightly as in the low-fluence case. However, this overshoot is masked during the first picosecond by the longer exponential recovery of the initial signal.

Figure 1(d) shows the dielectric function changes corresponding to the high-fluence data. The sign and ratio of magnitudes of the initial $\Delta\epsilon_1/\epsilon_1$ and $\Delta\epsilon_2/\epsilon_2$ closely resemble the low-fluence case. Strong interband saturation over a wide spectral range is expected at this pump fluence. The relationship between interband saturation and the optical response is discussed in Section IV.

Further insight into the initial optical transient was obtained by probing the front-surface reflectivity of a bulk HOPG sample with white-light continuum (0.45 μm $<\lambda_{\text{probe}}<0.84$ μm) or second harmonic ($\lambda_{\text{probe}}=0.31$ μm) pulses. Thin-film transmission data were not taken with a white-light or second-harmonic probes. However, to a good approximation, the bulk reflectivity changes in graphite can be interpreted in the context of an interband saturation model, as discussed further in Sec. IV. This approximation is based on our numerical estimates $\partial R/\partial\epsilon_1=-0.003$ and $\partial R/\partial\epsilon_2=0.024$ for small bulk reflectivity changes in HOPG. Since the thin-film measurements at 620 nm for high-fluence [Fig. 1(d)] show that $\Delta\epsilon_1$ and $\Delta\epsilon_2$ are of the same order of magnitude, we assume that the bulk reflectivity change $\Delta R/R_0$ at other probe wavelengths is dominated by changes in ϵ_2.

Figure 2 presents time-resolved reflectivity curves for the first picosecond of time delay for five different probe

wavelengths in the range $0.45\ \mu m < \lambda < 0.84\ \mu m$ from a white-light continuum probe, with pump fluence at 13 mJ/cm^2. The data in Fig. 2 were all taken with the pump-and-probe beams on the same spot on one sample.

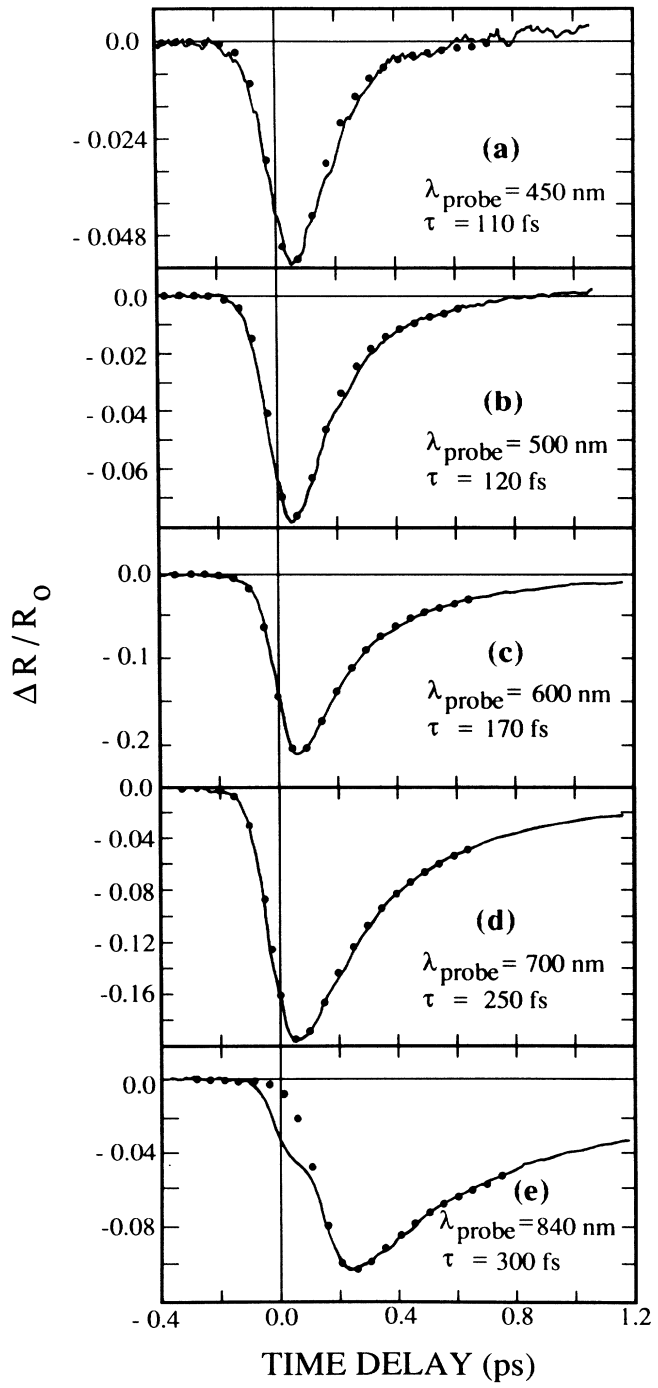

FIG. 2. Femtosecond reflectivity data from bulk graphite taken with amplified 50-fs pump pulses and white-light continuum ($0.45\ \mu m < \lambda_{probe} < 0.84\ \mu m$) probe pulses, showing the first picosecond of the optical response. Pump fluence was 13 mJ/cm^2. Dots are fits to the data of an exponential response function convolved with Gaussian pump and probe temporal profiles. Note that the exponential time constant τ is longer for longer probe wavelengths.

In all cases an initial reflectivity drop occurs, as was observed with the 620-nm probe. However, close inspection of the wavelength dependence reveals several additional trends. First, there is a monotonic increase in the decay time constant of the initial transient as probe wavelength increases from 0.45 to 0.84 μm. The dots represent fits of the data to a single exponential convolved with pump-and-probe temporal profiles. The time constant τ increases from 110 fs at $\lambda_{probe}=0.45\ \mu m$ to 300 fs at $\lambda_{probe}=0.84\ \mu m$, as marked on each panel in Fig. 2. The pump-probe cross-correlation curves obtained by sum frequency absorption in ZnO have a narrower temporal width, a completely different (symmetric, nonexponential) temporal shape, and a completely different dependence on probe wavelength than these observed optical responses. Therefore, the observed monotonic increase in recovery time with λ_{probe} is an intrinsic feature of the sample response, unrelated to details of the continuum generation process. Also, the magnitude of the initial reflectivity transient depends on probe wavelength, the largest ΔR peak occurring at probe wavelengths near the pump wavelength. The unusual "kink" in the falling edge of the 840-nm curve [Fig. 2(e)] has no counterpart in lower-fluence data [Fig. 3(e)] or in cross-correlation curves. It is therefore believed to be a real part of the high-fluence optical response, related to the optical saturation process, although its precise physical origin is not understood.

Figure 3 shows reflectivity data at the same probe wavelengths, but at a pump fluence of 1.3 mJ/cm^2. The time constant is smaller at each λ_{probe} compared to the higher fluence. Nevertheless, the wavelength dependence of ΔR and τ of the initial reflectivity transient closely resembles that observed at higher fluence. This wavelength dependence reinforces the picture of absorption saturation caused by a dense, rapidly relaxing electron-hole plasma, as described in detail in the following section.

Figure 4 illustrates the behavior of the reflectivity signals beyond the first picosecond for pump fluence of 13 mJ/cm^2. Figure 4(a) shows reflectivity data at $\lambda_{probe}=0.31\ \mu m$ (second harmonic) over a 6-ps interval. The initial drop in reflectivity (-1.7%) is much weaker than at longer λ_{probe}, and recovers more rapidly, consistent with the trends in wavelength dependence observed with the white-light continuum probe (Figs. 2 and 3). A unique feature of the uv reflectivity, however, is the sharp ($+4\%$) increase with a rise-time constant $\tau \sim 1$ ps which occurs after this initial transient. This increased reflectivity was observed to relax slowly with a time constant $\tau \sim 500$ ps. We believe that this increased uv reflectivity is caused by lattice heating, and the accompanying downward shift in the energy of the main oscillator peak of the π-electron band, as discussed in Sec. IV.

A 10-times-smaller reflectivity increase at $\Delta t > 1$ ps is observed at $\lambda_{probe}=0.45\ \mu m$ [Fig. 4(b)], and progressively smaller increase at $\lambda_{probe}=0.50\ \mu m$ [Fig. 4(c)] and 0.62 μm [see Fig. 1(a)]. For $\lambda_{probe} > 0.65\ \mu m$ [Figs. 4(d) and 4(e)], no reflectivity increase was observed at all at $\Delta t > 1$ ps, the initial negative transient recovering exponentially to $\Delta R/R_0 = 0$. At $\lambda_{probe}=0.62\ \mu m$, the weak positive

overshoot was followed out to long time delays, and observed to behave differently from the 0.31-μm signal. It slowly relaxed over a time interval of approximately 17 ps, corresponding to a time constant of 5 ps, then reached a maximum negative value at $\Delta t \sim 25$ ps, approximately one-tenth the magnitude of the maximum positive value, before beginning a much slower recovery. Thus the physical origin of this signal may differ from that of the 0.31-μm signal. Nevertheless, we believe that this positive overshoot in $\Delta R/R_0$ corresponds to the initial positive reflectivity transient reported by Heremans *et al.*[7] in a time-resolved reflectivity experiment on HOPG using 5-ps pulses with $\lambda_{probe}=0.5925$ μm. Because of the longer pulse duration, the rapid initial negative reflectivity transient was not resolved in that experiment.

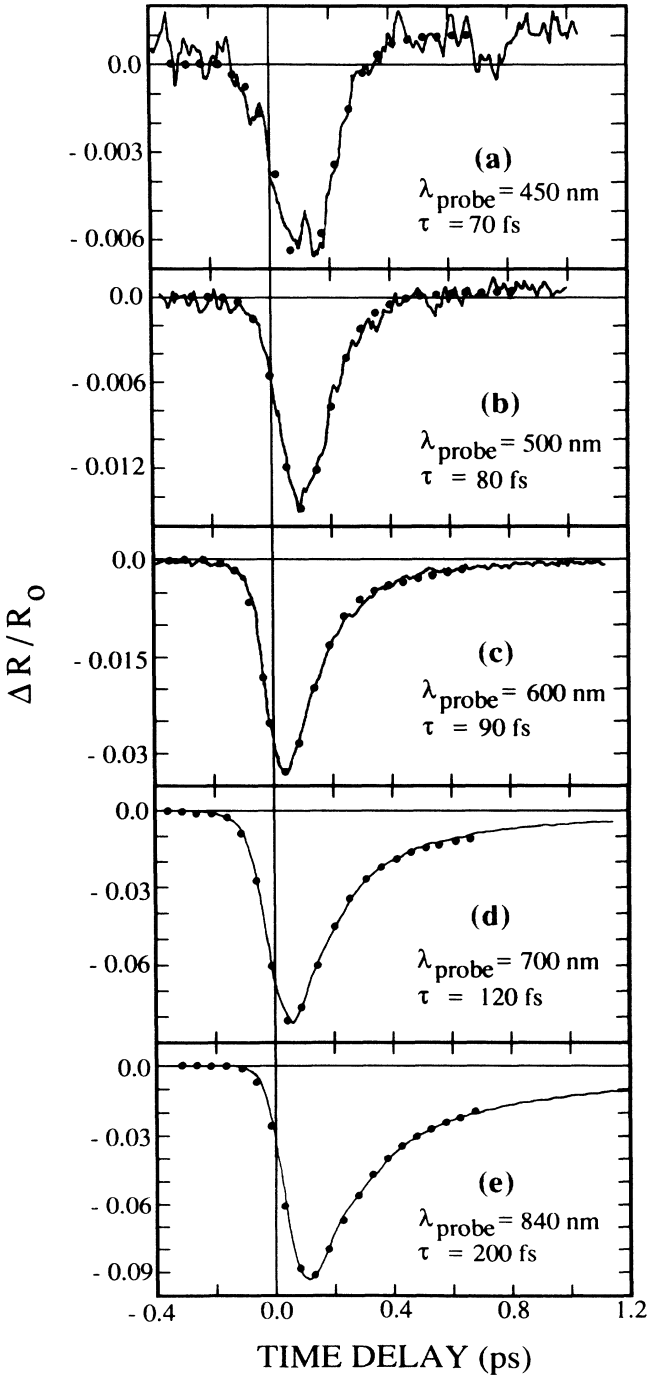

FIG. 3. Femtosecond reflectivity data from bulk graphite as in Fig. 2, but with pump fluence 1.3 mJ/cm^2.

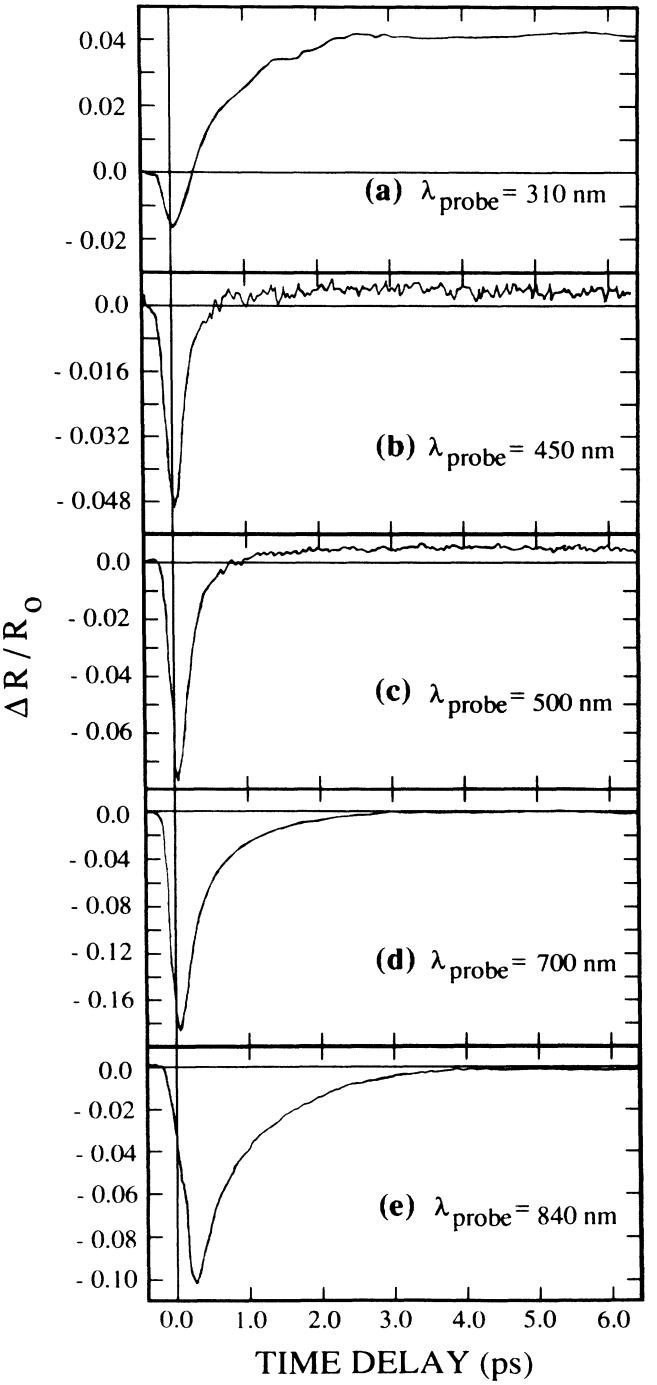

FIG. 4. Femtosecond reflectivity data from bulk graphite, showing the optical response beyond the first picosecond. Pump fluence was 13 mJ/cm^2, probe pulses were (a) second-harmonic or (b)–(e) white-light continuum pulses. Note that the positive $\Delta R/R_0$ signal for $\Delta t > 1$ ps is larger for shorter probe wavelengths.

IV. DISCUSSION

A. Carrier dynamics during the first picosecond

In this section we present a simple model of interband absorption saturation caused by carrier generation, and relate the time evolution of this saturation to the observed reflectivity and transmission changes shown in Fig. 1–3. The general concept of absorption saturation can be understood at the simplest level by considering the interaction of light with a two-level system consisting of ground state "a" and excited state "b", each of which can be multiply populated. Optical absorption consists of the partial promotion of population in state "a" to state "b" by the absorption of photons at the resonant frequency ω_{ba}. Therefore the optical absorption coefficient of such a "sample" is proportional to the population difference $N_b - N_a$ between the excited and ground states. If the population of the two states becomes equal, the absorption coefficient drops to zero, corresponding to complete absorption "saturation." Absorption of a strong resonant pump pulse will partially saturate the system's absorption (and therefore increase its transmission) for a closely following resonant probe pulse by temporarily reducing the population difference between, and therefore the absorption coefficient corresponding to, the two states.

In order to apply this general concept to analysis of our data, we must use the actual energy levels of HOPG which occur at energy separations corresponding to the experimental pump-and-probe frequencies. The optical properties of graphite below 8 eV are determined almost entirely by the π-electron bands,[3,4] which arise from the one electron per atom originating in the atomic $2p_z$ orbitals extending above and below the carbon layer planes. The experimental results can therefore be discussed in terms of generation and relaxation of carriers entirely within the π bands. Figure 5 depicts a portion of the π bands near the band extrema located at one corner of the hexagonal Brillouin zone (K point), showing the valence- and conduction-band states coupled by 2.0-eV pump photons. Initially, carriers are generated in the optically coupled states, as shown schematically by the electron and hole distributions labelled "τ_1." These carriers then thermalize nearly instantaneously by carrier-carrier scattering, spreading the distributions over a wide energy range both above and below the optically coupled states, as illustrated by distributions "τ_2." This hot-carrier population causes absorption saturation not only at 2.0 eV, as in the Fig. 1 data, but to a lesser extent at probe wavelengths widely separated from the pump, as in Figs. 2 and 3.

The wavelength dependence of the decay time constant in the Fig. 2 data is explained by the subsequent relaxation of the initial carrier distribution. As carriers transfer energy to the lattice via the electron-phonon interaction, electrons and holes relax toward the respective band extrema, reaching distributions such as those labeled "τ_3." Consequently, absorption saturation recovers more rapidly at probe wavelengths shorter than the pump, since carriers relax more rapidly out of states farther from the band extrema. On the other hand, saturation persists at longer probe wavelengths, because initially higher-energy carriers relax into lower-energy states coupled by these wavelengths. The fluence dependence of the relaxation time is also consistent with this picture, because at higher carrier density a wider initial energy spread is expected. Thus optically generated carriers require more time to relax from higher-energy into lower-energy optically coupled states via electron-phonon scattering processes. The displacement of the peak signals from $\Delta t = 0$ shows that the signal depends on accumulation of carriers throughout the pump temporal profile, in contrast to a χ^3 effect which would follow the pump-intensity profile. In principle, a slight increase in this displacement with increasing recovery time τ is expected. However, our experimental uncertainty in determining $\Delta t = 0$ (approximately ± 20 fs) is too great for this increase to be clearly evident in the data.

The equality of the recovery time constant in R and T shows that vertical carrier diffusion plays a negligible role during the first few picoseconds. $\Delta R/R_0$ is determined by carrier density at the front surface, and is therefore sensitive to vertical diffusion; $\Delta T/T_0$, on the other hand, depends on integrated carrier density across the sample thickness, and is therefore insensitive to carrier diffusion. This result has been confirmed also in thicker ($L \sim 600$ Å) samples. For an absorption depth of 300 Å at 2.0 eV,[3,4]

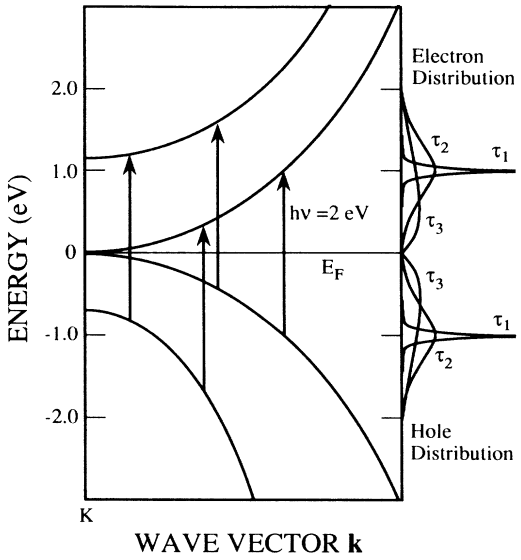

FIG. 5. Partial π band-structure diagram of graphite adapted from the calculation of Johnson and Dresselhaus (see Ref. 4) showing occupied, bonding valence bands and unoccupied, antibonding conduction bands near the corner of the hexagonal Brillouin zone (K point). The Fermi energy E_F is defined as the zero of energy. The arrows illustrate interband optical excitation at a photon energy $h\nu = 2.0$ eV. The initial electron and hole distributions, represented schematically by the curves labeled "τ_1," thermalize rapidly by carrier-carrier collisions to broader distributions, represented schematically by the curves labeled "τ_2." Within a few hundred femtoseconds, the hot carriers relax toward the band extrema, reaching distributions such as those labeled "τ_3."

this places an upper limit of $D \sim 1$ cm^2/s on the ambipolar diffusion coefficient for our sample, consistent with the lower end of the range of values reported for pyrolytic graphite samples.[1]

By examining the electronic density of states, we can formulate a quantitative, although approximate, model of the evolution of the carrier-density distribution in HOPG. To a good approximation, the density of π-electronic states within 1 eV of the band extremum can be written as[17]

$$D_\pi(E)=4|E|/9\pi d a^2\gamma_0^2+16\gamma_1/9\pi^2 d\gamma_0^2 a^2 , \quad (1)$$

where $|E|$ is the energy separation from the band extremum, $d=3.35$ Å is the interlayer separation, $a=1.42$ Å is the nearest-neighbor atomic spacing, and γ_0 and γ_1 are band-structure parameters which have been given different values in different band-structure calculations[4,17–19] (typically $\gamma_0 \sim 2.5$ eV, $\gamma_1 \sim 0.3$ eV). Since most band-structure calculations have shown the valence and conduction bands to be nearly symmetric around $E=0$ within 1 eV of $E=0$, Eq. (1) can be assumed equally valid for both bands over the range of energies relevant for analyzing the experimental data. In discussions of optical properties, the band symmetry further implies that E can be assumed equal to $h\nu/2$, in which case Eq. (1) provides a good approximation to the joint density of states. Inserting numbers, the density of states (including spin degeneracy) of either band can be expressed as[20]

$$D_\pi(E)=[(7\pm3)\times10^{21}\ \text{eV}^{-2}\text{cm}^{-3}]E + (3\pm1)\times10^{21}\ \text{eV}^{-1}\text{cm}^{-3} . \quad (2)$$

The indicated uncertainties reflect the range of values of the parameters γ_0 and γ_1 which have been used in various band-structure calculations.[4,17–19] The effect of optical excitation is to create a carrier distribution $N(E)$, which causes interband absorption saturation by state filling. The degree of saturation which influences a probe at $h\nu$ at some instant is then proportional to the ratio $N(h\nu/2)/D_\pi(h\nu/2)$. We assume Drude contributions to the dielectric function to be small at visible and near-ultraviolet wavelengths. The fractional change in the imaginary part of the dielectric function can be expressed as

$$\Delta\epsilon_2(E)/\epsilon_2(E)=-N(E)/D_\pi(E) . \quad (3)$$

By deriving the ratio $\Delta\epsilon_2/\epsilon_2$ from optical data over a wide range of wavelengths and time delays, it then becomes possible, using Eqs. (2) and (3), to construct the carrier distribution $N(E)$ as it evolves on a femtosecond time scale. As an additional constraint on the distribution $N(E)$, the initial integrated carrier density must equal the total carrier density generated by absorption of the pump pulse of fluence F with absorption coefficient $\alpha(h\nu_{\text{pump}})$. As long as absorption saturation and multiphoton are weak, this constraint can be expressed as

$$\int_0^\infty N(E)\,dE=(1-R)F\alpha/h\nu . \quad (4)$$

At $h\nu_{\text{pump}}=2.0$ eV, $R=0.32$ and $\alpha=3\times10^5$ cm^{-1}. Therefore at $F=1.3$ mJ/cm^2, a total initial carrier density 8×10^{20} cm^{-3} is expected, while at $F=13$ mJ/cm^2, a total density of 8×10^{21} cm^{-3} is expected. If recombination remains negligible on the time scale of the experiment, then the relation (4) remains valid for all time delays as the distribution $N(E)$ evolves.

In cases where both transmission and reflectivity data are available, the fractional change $\Delta\epsilon_2/\epsilon_2$ required to derive $N(E)$ can be determined without any approximations. For example, from the data in Fig. 1(c) and the analysis in Fig. 1(d), we obtain $\Delta\epsilon_2(h\nu=2.0\ \text{eV})/\epsilon_2(h\nu=2.0\ \text{eV})=-0.28$ at the peak, yielding $N(E=1.0\ \text{eV})=2.4\times10^{21}\ \text{eV}^{-1}\text{cm}^{-3}$ from Eqs. (2) and (3). Furthermore, we have verified at several pump fluences that ϵ_1 and ϵ_2 derived from a thin-film measurement account for the front surface reflectivity response of a bulk sample at $h\nu_{\text{probe}}=2.0$ eV to within 10%. In order to construct $N(E)$ at other energies, however, we must analyze data taken with different $h\nu_{\text{probe}}$. Since only reflectivity data are available (Figs. 2 and 3), an additional assumption is required to relate $\Delta\epsilon_2(h\nu)/\epsilon_2(h\nu)$ to the observed $\Delta R(h\nu)/R(h\nu)$. We shall assume, once $\Delta\epsilon_2/\epsilon_2$ is determined at $h\nu=2.0$ eV from thin-film measurements, that $\Delta\epsilon_2/\epsilon_2$ is simply proportional to the measured $\Delta R/R$ at $h\nu_{\text{probe}}\neq2.0$ eV. Although only approximately correct, this assumption is expected to introduce less error into the derived values of $N(E)$ than uncertainties in the value of the electronic density of states $D_\pi(E)$. The value of $N(h\nu/2)=-\Delta\epsilon_2(h\nu)/\epsilon_2(h\nu)^* D_\pi(h\nu/2)$ for each probe photon energy $h\nu$ is then derived using Eqs. (2) and (3).

Figure 6 presents the results of such an analysis for the reflectivity data in Fig. 3, for which $F_{\text{pump}}=1.3$ mJ/cm^2. Although no reflectivity data were taken at $h\nu_{\text{probe}}>1.48$ eV, the results suggest that, immediately after the pump is absorbed ($\Delta t=100$ fs), $N(E)$ is maximum just below

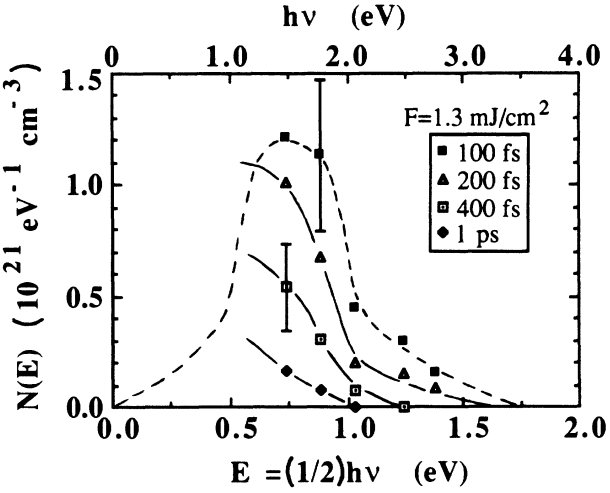

FIG. 6. Carrier energy distributions at four different time delays following a 2.0-eV pump pulse at fluence $F=1.3$ mJ/cm^2, derived from optical reflectivity data in Fig. 3 as explained in text. The plotted points represent densities inferred directly from the data. The dashed curve is a Maxwell distribution with an integrated carrier density of 8×10^{20} cm^{-3}, which corresponds to $(1-R)F\alpha/h\nu$.

the optically pumped states at $E=h\nu/2=1.0$ eV. A Maxwellian (solid) curve centered at $E=0.8$ eV has been drawn through the available data points for $\Delta t=100$ fs, in accordance with the expectation that carrier-carrier scattering processes rapidly thermalize the optically generated nondegenerate plasma. Significantly, the area under this Maxwellian curve — i.e., the integrated carrier density $(1-R)F\alpha/h\nu=8\times10^{20}$ cm^{-3} determined independently from the known pump fluence — satisfies criterion (4). This good agreement demonstrates the internal consistency of the above analysis, and supports the assumption that the observed optical response is indeed caused primarily by absorption saturation. Because of band symmetry the curve represents both the electron and hole distributions. The representative error bars shown reflect uncertainties in the value of the electronic density of states equation (2). The other curves in Fig. 6 represent similar analyses of the Fig. 3 reflectivity data at later time delays. The center of the distribution moves toward lower energy, as expected for a hot plasma relaxing via electron-phonon scattering processes. Increasingly the experimental probe wavelengths sample only the high-energy tail of the distribution as relaxation proceeds.

Figure 7 presents similarly derived carrier distribution curves for a pump fluence $F=13$ mJ/cm^2, based on the reflectivity data in Fig. 2. At $\Delta t=100$ fs, the experimentally determined $N(E)$ is strongly peaked near the energy $E=h\nu/2=1.0$ eV corresponding to the optically pumped states. However, it is not possible to draw a smooth curve through the experimental points with an area $F\alpha/h\nu=8\times10^{21}$ cm^{-3} without introducing an unphysical distortion in the low-energy part of the curve. In fact, the area under the curve drawn in Fig. 7 corresponds to a total density of only 3×10^{21} cm^{-3}. This discrepancy probably results from strong absorption saturation at this fluence. Indeed, using the density-of-states function (2), the integral $\int D_\pi(E)\,dE$ from 0 to 1 eV yields 6.5×10^{21} cm^{-3}, which is the maximum density of carriers which can be generated even with complete band filling. The leading edge of the pump pulse thus increases the effective absorption depth α^{-1} for the trailing edge, spreading the generated carriers over a larger volume. Indeed, the Fig. 1(c) data show a 40% transmission increase during a pump pulse of 7.5 mJ/cm^2. It is therefore reasonable to expect that the effective α^{-1} could be doubled at 13 mJ/cm^2. Furthermore at this high pump fluence, the simple relationship (3) between state filling and the dielectric function may no longer be a good approximation, as free-carrier absorption, X^3 effects, and other nonlinear-optical processes become important. In view of these complications, the $N(E)$ curves in Fig. 7 should be regarded as rough approximations only. Nevertheless, the derived curves show that at later time delays $N(E)$ again shifts toward lower energy, although a peak near $h\nu=2$ eV persists for half a picosecond. For $\Delta t=200$ and 400 fs, we find that completion of smooth curves through the experimental points requires progressively smaller integrated area than the $\Delta t=100$ fs curve. The $\Delta t=200$ fs curve corresponds to a density of 1.75×10^{21} cm^{-3} and the $\Delta t=400$ fs curve to a density of 1×10^{21} cm^{-3}, nearly the density generated at 10-times-lower fluence. This decreasing area suggests that a density-dependent recombination process may become important at these high densities. However, because of the complications involved in interpreting the high-fluence data, we do not believe that more detailed analysis of this recombination is justified at this time.

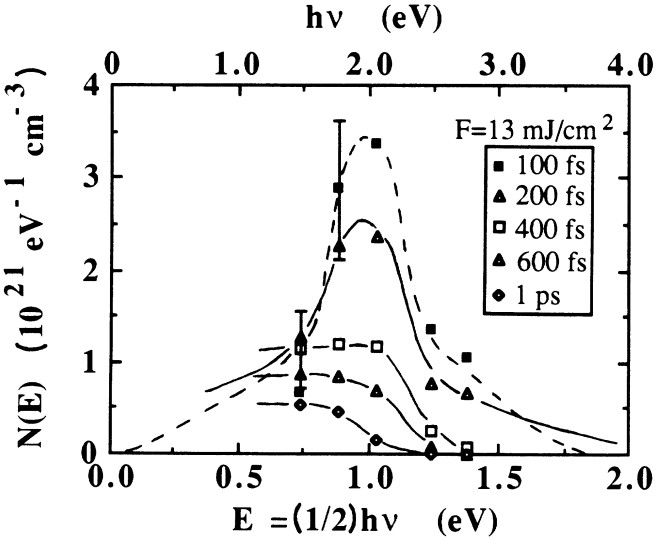

FIG. 7. Carrier energy distributions as in Fig. 6, but for pump fluence $F=13$ mJ/cm^2.

B. Dynamics beyond the first picosecond

The most striking effect observed beyond the first picosecond is the pronounced uv reflectivity rise shown in Fig. 4(a). The rise time of this signal ($\tau\sim1$ ps) is consistent with the time required for the lattice to heat as optically excited electron-hole pairs relax to the band extrema via phonon emission. Furthermore, the observed fall time (~500 ps) is consistent with the expected time for vertical thermal diffusion under our experimental conditions. This time is estimated from the expression

$$\tau_{\text{thermal}}\sim1/\alpha^2D=\rho C_p/\kappa\alpha^2\sim550\text{ ps},$$

where the optical-absorption coefficient $\alpha=3\times10^5$ cm^{-1} at the pump wavelength 620 nm,[4] and the thermal diffusion coefficient $D=0.017$ cm^2 s^{-1} is determined from density $\rho=2.25$ g/cm^3, heat capacity $C_p=19.5$ J/mol K, and thermal conductivity $\kappa=0.06$ J/cm s K for pyrolytic graphite[9] at the final temperature $T=300$ K$+F(1-R)\alpha/\rho C_p\sim1000$ K of the sample surface after pumping at $F=13$ mJ/cm^2. These features of the uv reflectivity rise provide strong evidence that it is caused by lattice heating.

The uniqueness of this signal to the ultraviolet probe is explained by the unique position which 4.0-eV light probes in the band structure of graphite, as illustrated by the partial graphite reflectivity spectrum in Fig. 8. The 4.0-eV light probes the steeply sloped low-energy edge of the main oscillator peak of the π bands, which arises

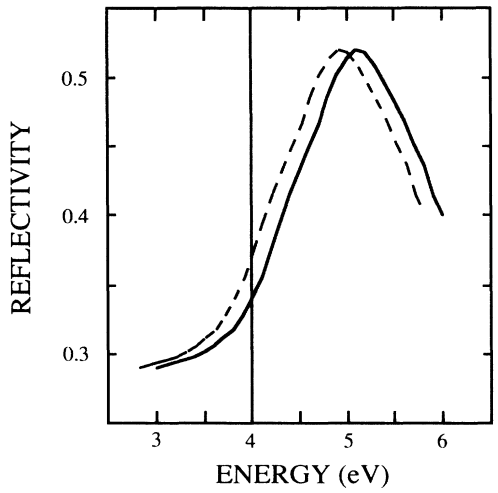

FIG. 8. Partial reflectivity spectrum of HOPG (solid curve) showing the main oscillator peak of the π bands. Dashed curve represents shifting of the reflectivity peak caused by lattice heating, inducing a strong reflectivity rise at $h\nu = 4$ eV.

from a large joint density of states at energy separation 4.2 eV which occurs near the corner of the Brillouin zone.[4] Thus the reflectivity of 4.0-eV light is highly sensitive to small shifts in this band separation, but insensitive to the interband saturation effects which dominate the optical response of visible and near-infrared probes (as with visible probes, Drude effects are negligible at ultraviolet probe wavelengths). Indeed, as lattice temperature rises, shrinkage of this band separation, analogous to thermal band-gap shrinkage in semiconductors, is expected. A downward shift (assuming no broadening) of only 0.1 eV in the energy of this peak is sufficient to explain the 4% rise in uv reflectivity observed at a pump fluence of 13 mJ/cm^2, as illustrated by the dashed line in Fig. 8. The magnitude of this shift is comparable to thermal band-gap shrinkages observed in semiconductors for similar temperature rises.[21] In contrast, the visible wavelength probes fall in a relatively flat portion of the reflectivity spectrum, and are therefore insensitive to shifts in the band energies. Thus the visible and ultraviolet probes provide complementary diagnostics of different aspects of the ultrafast dynamics of graphite.

The uv reflectivity data show no evidence of electronic band renormalization induced by the presence of a high electron-hole–pair density. The effects of such renormalization would be expected to occur immediately upon injection of carriers, rather than after a 1-ps delay as observed in our experiment. We must therefore conclude that electronic band renormalization is a much weaker effect than thermal band shrinkage in graphite. By contrast, band-gap shifts as large as 0.5 eV induced by carrier densities of 10^{21} cm^{-3} are observed and calculated in many semiconductors.[22] However, no previous observations or theories of this effect in graphite are available. The apparent weakness of electronic band renormalization may be a unique property of graphite or of the particular band separation probed by our experiment.

The much smaller reflectivity increases observed after $\Delta t = 1$ ps at $\lambda_{\text{probe}} = 450$ and 500 nm [Figs. 4(b) and 4(c)] may also be caused by the shift of the oscillator peak observed in its long-wavelength tail. However, the time dependence of these signals was not investigated at time delays $\Delta t > 7$ ps. The relatively rapid (~ 20 ps) recovery of the small reflectivity increase at $\lambda_{\text{probe}} = 620$ nm, on the other hand, suggests that this signal has a different physical origin. This signal may be caused by the degenerate electron-hole plasma near the band extrema following relaxation of the plasma. Indeed, state filling (absorption saturation) near the band extrema should yield a small reflectivity increase for photons probing unoccupied states at higher energies in the band, according to the Kramers-Kronig relation. The recovery of the signal could then be ascribed to electron-hole recombination. The rapid time scale of recombination compared to direct-band-gap semiconductors could be attributed to the absence of a band gap, which permits recombination without the requirement of photon or phonon emission to conserve energy and momentum. Carrier diffusion may also play a role, although the exponential shape of the recovery is not consistent with a diffusion model. Indeed diffusion along the c axis is expected to be slow in a quasi-two-dimensional structure such as graphite.

V. CONCLUSION

A comprehensive study of femtosecond carrier dynamics in a quasi-two-dimensional semimetallic solid has been performed using femtosecond reflectivity and transmission measurements on graphite. Experimental results were analyzed using a model based on absorption saturation caused by state filling by a dense, nonequilibrium electron-hole population, which was used to reconstruct the hot-carrier energy distribution as it evolves on a subpicosecond time scale. Carrier dynamics during the first picosecond resemble dynamics observed in direct-band-gap semiconductors.[23] Initially a hot, nondegenerate plasma is created at energies corresponding to the optically pumped states, and is thermalized by carrier-carrier scattering processes on a time scale shorter than the resolution of our experiment. The electron and hole distributions then relax to the respective band extrema by electron-phonon scattering processes in approximately 1 ps. At very high carrier densities, evidence of density-dependent recombination is observed on this time scale. These measurements provide essential input for theories of the electronic and optical properties of graphite, which require knowledge of fundamental scattering times which have not previously been measured.

ACKNOWLEDGMENTS

Two of us (A.M.M and M.C.D.) gratefully acknowledge financial support from Rheinisch-Westfälische Technische Hochschule Aachen during the experimental phases of this work. Two of us (M.C.D. and D.H.R.) also acknowledge the support of the U.S. National Science Foundation (Grant No. DMR-88-58388), the U.S. Air Force Office of Scientific Research (Contract No. F49620-89-C-0044), and the Robert A. Welch Foundation (Grant F-1038), Houston, TX for work performed at the University of Texas.

[1]B. T. Kelly, *Physics of Graphite* (Applied Science, London, 1981).

[2]P. R. Wallace, Phys. Rev. **71**, 622 (1947).

[3]E. A. Taft and H. R. Philipp, Phys. Rev. **138**, 197 (1965).

[4]L. G. Johnson and G. Dresselhaus, Phys. Rev. B. **7**, 2275 (1973).

[5]*Ultrafast Phenomena VI,* edited by T. Yajima, K. Yoshihara, C. B. Harris, and S. Shionoya (Springer, Heidelberg, 1988).

[6]A. M. Malvezzi, N. Bloembergen, and C. Y. Huang, Phys. Rev. Lett. **57**, 146 (1986); A. M. Malvezzi, G. Reverberi, and N. Bloembergen, in *Fundamentals of Beam-Solid Interactions and Transient Thermal Processing, 1987,* Vol. 100 of *Materials Research Society Symposia Proceedings,* edited by M. J. Aziz, L. E. Rehn, and Bernd Stritzker (Materials Research Society, Pittsburgh, 1988), p. 483.

[7]J. Heremans, C. H. Olk, G. L. Eesley, J. Steinbeck, and G. Dresselhaus, Phys. Rev. Lett. **60**, 452 (1988).

[8]T. Venkatesan, D. C. Jacobson, J. M. Gibson, B. S. Elman, G. Braunstein, M. S. Dresselhaus, and G. Dresselhaus, Phys. Rev. Lett. **53**, 360 (1984).

[9]J. Steinbeck, G. Braunstein, M. S. Dresselhaus, T. Venkatesan, and D. C. Jacobson, J. Appl. Phys. **58**, 4374 (1985).

[10]E. A. Chauchard, Chi H. Lee, and C. Y. Huang, Appl. Phys. Lett. **50**, 812 (1987).

[11]J. Steinbeck, G. Braunstein, J. Speck, M. S. Dresselhaus, C. Y. Huang, A. M. Malvezzi, and N. Bloembergen, in *Beam-Solid Interactions and Transient Processes, 1986,* Vol. 14 of *Materials Research Society Symposia Proceedings,* edited by M. O. Thomson, S. T. Picraux, and J. S. Williams (Materials Research Society, Pittsburgh, 1987), p. 263.

[12]D. H. Reitze, X. Wang, H. Ahn, and M. C. Downer, Phys. Rev. B **40**, 11 986 (1989).

[13]J. Valdmanis, R. L. Fork, and J. P. Gordon, Opt. Lett. **10**, 131 (1985).

[14]M. Strahnen, W. Kutt, and H. Kurz (unpublished).

[15]W. H. Knox, M. C. Downer, R. L. Fork, and C. V. Shank, Opt. Lett. **9**, 552 (1984).

[16]R. L. Fork, C. V. Shank, C. Hirlimann, R. Yen, and W. J. Tomlinson, Opt. Lett. **8**, 1 (1983).

[17]J. W. McClure, Phys. Rev. **104**, 666 (1956).

[18]L. C. Olsen, Phys. Rev. B **6**, 4836 (1972).

[19]H. Fukutani and G. Kuwabara, J. Phys. Soc. Jpn. **46**, 893 (1979).

[20]C. A. Coulson and R. Taylor, Proc. Phys. Soc. London, Sect. A **65**, 815 (1952).

[21]Y. P. Varshni, Physica (Amsterdam) **34**, 149 (1967).

[22]K. F. Berggren and B. E. Sernelius, Phys. Rev. B **24**, 1971 (1981).

[23]W. Kütt, K. Seibert, and H. Kurz, in *Ultrafast Phenomena VI,* edited by T. Yajima, K. Yoshihara, C. B. Harris, and S. Shionoya (Springer, Heidelberg, 1988), p. 233.